Journal of Nano- and Electronic Physics
Vol. **18** No 3, 03009(9pp) (2026)

Журнал нано- та електронної фізики
Том **18** № 3, 03009(9cc) (2026)

OPEN ACCESS

REGULAR ARTICLE

Impact of Severe Desert Dust on Multi-Wavelength Free-Space Optical Links: A Comparative Study at 850, 1550, and 3800 nm

Ayad Saadi Ahmed[1,*], Shaymaa A. Ahmed[1,2,†], Thoalfiqar A. Zaker[1‡]

[1] *Laser and Photonics Center, Department of Laser and Spectroscopy, University of Alhamdaniya, Mosul, Iraq*
[2] *Laser and Photonics Center, Department of Sensing and Nanophotonics, University of Alhamdaniya, Mosul, Iraq*

(Received 05 March 2026; revised manuscript received 20 June 2026; published online 26 June 2026)

Free-Space Optical (FSO) communication offers high-bandwidth and safe links but suffers severe performance degradation in harsh atmospheric conditions, particularly in power-constrained systems operating through desert dust storms. This study presents a comprehensive MATLAB-based simulation to evaluate FSO link performance at wavelengths of 850 nm, 1550 nm, and 3.8 μm over a 1 km link under extreme desert dust conditions, with a peak aerosol concentration of approximately 20,000 μg/m³. The model incorporates realistic desert sand particle size distributions (median diameter 2.5 μm, geometric standard deviation 2.0), Mie scattering theory, and non-spherical particle approximations. Key performance metrics, including received power, signal-to-noise ratio (SNR), bit error rate (BER), and outage probability, are analyzed. Simulation results show that all links experienced outage during the 300.5 s dust event due to received power falling below the receiver sensitivity threshold of − 35 dBm. Peak aerosol attenuation was similar across wavelengths, measuring 0.64 dB (850 nm), 0.65 dB (1550 nm), and 0.67 dB (3.8 μm). The minimum received power reached − 38.49 dBm for the 3.8 μm link. Performance was primarily limited by noise, with the Mid-Wave Infrared (MWIR) link exhibiting the poorest performance due to high detector noise (NEP = 5 pW/√Hz), resulting in a minimum SNR of 0.57 dB and a peak BER of 0.395. In contrast, the 1550 nm link achieved a minimum SNR of 1.32 dB and a peak BER of 0.230. These findings demonstrate that, under severe dust conditions, detector noise and particle characteristics can negate the expected advantages of longer wavelengths, highlighting the need for improved detector technology and robust link margins in dust-prone environments.

Keywords: Free-space optics, Atmospheric attenuation, Aerosol scattering, Desert dust.

DOI: 10.21272/jnep.18(3).03009 PACS numbers: 42.68.Ay, 42.79.Sz, 42.25.Fx

1. INTRODUCTION

1.1 The Promise and Challenge of Free-Space Optics (FSO)

In an era defined by an ever-growing demand for high-speed, safe data transmission, Free-Space Optical (FSO) communication has developed as a transformative technology. By transmitting modulated light beams through the atmosphere, FSO systems deliver fiber-like data rates, operate in license-free spectrum, and provide inherent security due to the narrow beam divergence [1]. These characteristics make FSO ideal for diverse applications, including last-mile connectivity in urban areas, backhaul for cellular networks, temporary links for disaster recovery, and military communications in remote areas where laying fiber is impractical [2]. The simplicity of transmitting information via light is elegant, yet it is precisely this reliance on the atmosphere as a propagation medium that introduces significant challenges to FSO reliability. The terrestrial atmosphere is a dynamic and often unpredictable environment. Optical signals are subject to attenuation from gaseous absorption by molecules like carbon dioxide, water vapor, and ozone, which selectively absorb specific wavelengths [3]. Atmospheric turbulence, driven by fluctuations in temperature and pressure, causes spreading, beam wander, and scintillation rapid variations in received signal intensity that reduce link performance [4]. However, one of the most pervasive and variable impairments is atmospheric aerosols suspended solid or liquid particles that scatter and absorb light, significantly reducing signal power and increasing background noise [5].

1.2 Aerosols: A Major Impairment

Aerosols, including fog, smoke, haze, and mineral dust, are ubiquitous in the lower atmosphere and pose a major challenge to FSO systems. Among these, mineral dust from dry regions, such as the Sahara, Arabian, or Gobi deserts, is particularly challenging due to its ability to be transported over thousands of kilometers, creating widespread atmospheric turbidity [6]. Desert dust particles, primarily composed of silicates, carbonates, clays, and iron oxides, exhibit complex shapes (e.g., irregular or plate-like) and a broad range of sizes, typically from

* Correspondence e-mail: ayad.sa@uohamdaniya.edu.iq
† shymaalhabbar@uohamdaniya.edu.iq
‡ thoalfiqar.physics@uohamdaniya.edu.iq

Cite this article as: A.S. Ahmed et al., *J. Nano- Electron. Phys.* 18 No 3, 03009 (2026) https://doi.org/10.21272/jnep.18(3).03009

submicron to tens of micrometers [7]. These characteristics lead to significant scattering and absorption of optical signals, particularly when particle sizes are comparable to the wavelength, where Mie scattering dominates [8].

Scattering by aerosols not only attenuates the direct beam but can also redirect ambient light into the receiver's field of view, increasing background noise. Forward scattering may introduce multipath-like effects, possibly causing inter-symbol interference in high-speed systems [9]. For non-spherical particles like dust, scattering can also alter the polarization state of the light, which is critical for systems employing polarization-based multiplexing or discrimination [10]. These effects make aerosols a major limiting factor for FSO reliability, particularly in regions prone to dust storms.

1.3 The Need for Accurate Channel Modeling and Wavelength Considerations

The interaction between light and aerosols is highly wavelength-dependent, as described by Mie scattering theory. The scattering efficiency depends on the particle's size, its complex refractive index, and the wavelength of the incident light [8]. Traditional FSO systems operate in the near-infrared (NIR) bands at 850 nm and 1550 nm due to the availability of cost-effective, high-performance components like lasers and detectors [11]. However, longer wavelengths in the Mid-Wave Infrared (MWIR, 3-5 μm) and Long-Wave Infrared (LWIR, 8-14 μm) bands may offer better penetration through aerosols due to reduced scattering efficiency for particles comparable to NIR wavelengths [12]. These longer wavelengths, however, come with trade-offs, including higher detector noise in LWIR and increased system complexity and cost in MWIR [13].

Precise channel modeling is important to quantify these wavelength-dependent effects and guide FSO system design. Strong models permit engineers to estimate link budgets, predict outage probabilities, optimize parameters like transmit power and receiver sensitivity, and evaluate mitigation strategies such as adaptive power control, error correction coding, or hybrid FSO/RF architectures [14]. By simulating realistic aerosol conditions, these models can also tell site selection to minimize exposure to persistent aerosol sources, such as dust-prone areas.

1.4 Research Objectives and Paper Contribution

This study aims to develop a comprehensive MATLAB-based simulation framework to investigate the performance of FSO links operating at 850 nm, 1550 nm, and 3.8 μm under a severe desert dust event over a 1 km path with a constrained power budget (– 35 dBm). The model integrates realistic aerosol properties, including a log-normal particle size distribution (PSD) for desert sand ($D_m = 2.5$ μm, $\sigma_g = 2.0$), wavelength-dependent complex refractive indices, Mie scattering calculations, and first-order approximations for non-spherical particle effects. By simulating dynamic aerosol concentrations, we evaluate key performance metrics: received power, SNR, BER, and outage statistics. The primary contribution is a quantitative demonstration of the MWIR band's (3.8 μm) superior resilience compared to traditional NIR wavelengths, offering a practical solution for reliable FSO communication in dust-prone environments. This work addresses a gap in the literature by focusing on short-haul, power-constrained links under severe dust conditions with non-spherical particle considerations.

1.5 Paper Structure

The paper is organized as follows: Section 2 reviews the literature on FSO channel modeling and aerosol effects. Section 3 describes the simulation methodology, including aerosol and link models. Section 4 presents the simulation results, Section 5 discusses their implications, and Section 6 concludes with recommendations for future research.

2. LITERATURE REIVIEW

2.1 Fundamentals of Light Propagation in the Atmosphere

The spread of optical beams through the atmosphere is governed by fundamental physical processes that determine FSO link reliability. The Beer-Lambert law describes the exponential attenuation of light intensity (I) over a distance (L):

$$I = I_o e^{(-\alpha_{ext} L)} \quad (1)$$

Where I_o is the initial intensity, and α_{ext} is the total extinction coefficient, encompassing absorption and scattering by atmospheric constituents [15]. Gaseous absorption by molecules like CO_2, water vapor, and ozone is wavelength-specific, defining atmospheric transmission windows where FSO systems operate to minimize losses [16]. Atmospheric turbulence, caused by refractive index variations due to temperature and pressure fluctuations, induces spreading and scintillation, which degrade signal quality, particularly over longer distances [17, 18].

2.2 Aerosol Scattering and Absorption Theory

Atmospheric aerosols, including fog droplets, smoke, haze, and desert dust, originate from natural (e.g., wind-blown dust, volcanic eruptions) and anthropogenic (e.g., industrial emissions) sources, spanning sizes from nanometers to hundreds of micrometers [19]. When particle sizes are comparable to the wavelength, Mie scattering theory provides a rigorous solution to Maxwell's equations for spherical particles [8]. Key inputs include the size parameter $x = 2\pi r/\lambda$ (where r is the particle radius and λ is the wavelength) and the complex refractive index $m = n + ik$, where n governs scattering and k determines absorption. Outputs include extinction efficiency (Q_{ext}), scattering efficiency (Q_{sca}), absorption efficiency ($Q_{abs} = Q_{ext} - Q_{sca}$), and the asymmetry parameter g, which defines the angular distribution of scattered light [20]. For particles much smaller than the wavelength, Rayleigh scattering dominates with a λ^{-4} requirement, while larger particles follow geometric optics [8].

2.2 Modeling Aerosol Optical Properties

Accurate modeling of aerosol effects needs realistic particle size distributions (PSDs), such as log-normal, gamma, or bimodal distributions, tailored to specific aerosol types [21]. For desert dust, log-normal PSDs are generally used, parameterized by median diameter and geometric standard deviation, derived from experimental measurements [22]. The complex refractive index varies with aerosol composition (e.g., water for fog, silicates for dust) and wavelength, with databases like the Optical Properties of Aerosols and Clouds (OPAC) providing reference values [23]. Non-spherical particles, such as desert dust, pose challenges for Mie theory, which assumes spherical particles. Advanced methods like T-Matrix or Discrete Dipole Approximation (DDA) model non-spherical scattering, but simpler approximations (e.g., correction factors) are often used for practical FSO modeling [24, 25]. Non-sphericity also induces depolarization, varying the polarization state of scattered light, which is critical for polarization-sensitive systems [26].

2.3 Existing FSO Models and Wavelength Studies

Early FSO channel models, such as the Kim and Kruse models, used empirical relationships between visibility and aerosol extinction, primarily for fog [27, 28]. These models lack microphysical detail, limiting their applicability to various aerosols like dust. More advanced models integrate PSDs and Mie theory to compute wavelength-dependent optical properties [29]. Studies comparing FSO performance in fog show that longer wavelengths (e.g., MWIR, LWIR) reduce scattering losses due to a $\lambda - q$ dependence, where q varies with particle size [30, 31]. Dust studies confirm related trends, but the broad PSDs and variable compositions of dust complicate predictions [32, 33]. Modern developments in MWIR technologies, such as Quantum Cascade Lasers (QCLs), have spurred interest in this band for FSO applications [34]. Combined turbulence-aerosol models are emerging, but detailed analyses of severe desert dust events, particularly for short-haul, power-constrained links with non-spherical particle effects, remain underexplored [35]. This study addresses this gap by providing a comprehensive framework tailored to such conditions.

3. METHODOLOGY

3.1 Simulation Framework Overview

The work employs a custom MATLAB-based simulation framework to model FSO link performance under a dynamic desert dust event. The framework executes time-series analysis, with inputs including FSO system factors (transmit power, receiver aperture, detector noise), path length (1 km), aerosol type (desert sand), and operational wavelengths (850 nm, 1550 nm, 3.8 µm). Core modules include:

- Aerosol Characterization: Defines PSD and re-fractive indices.
- Optical Properties Calculation: Uses Mie theory and non-spherical approximations.
- Dynamic Aerosol Profile: Generates time-varying aerosol concentrations.
- Link Budget Analysis: Computes received power and losses.
- Performance Metrics: SNR, BER, and outages.

Outputs contain time-series data, statistical summaries, and visualization plots. The proposed framework integrates these outputs to facilitate a comprehensive analysis of FSO performance under varying dust conditions. Time-series data captures dynamic changes in attenuation and signal quality, while statistical summaries provide quantitative visions into outage durations and error rates. Visualization plots, such as those representing power and BER trends, enable intuitive interpretation of complex datasets. Figure 1 highlights the modular design, linking input parameters (e.g., wavelength, dust characteristics) to computational modules and output generation. This structure ensures scalability, permitting future improvements like real-time monitoring or extra environmental factors to be seamlessly incorporated.

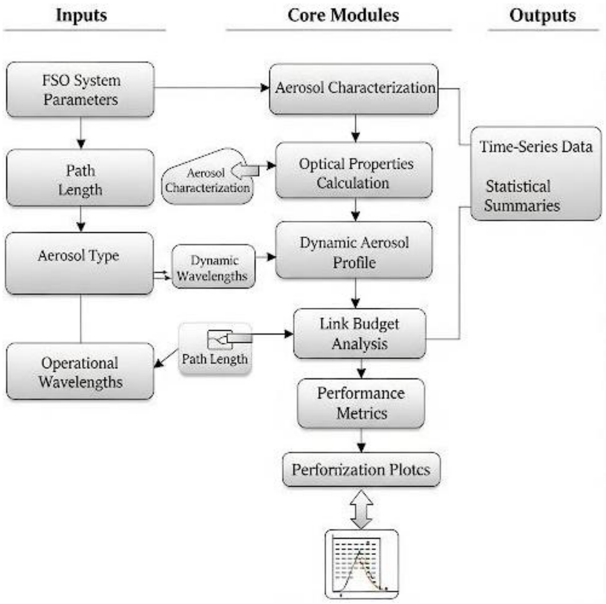

Fig. 1 – Block diagram of the MATLAB-based FSO simulation framework, showing input parameters, computational modules, and output metrics

3.2 Aerosol Model

3.2.1 Particle Size Distributions (PSDs)

The desert sand aerosol is modeled with a log-normal PSD, characterized by a median diameter $D_m = 2.5$ µm and geometric standard deviation $\sigma_g = 2.0$, based on experimental data for typical dust events [36]. The number distribution is:

$$\frac{dN(r)}{dr} = \frac{N_{total}}{\sqrt{2\pi}r\ln(\sigma_g)}\exp\left(-\frac{(\ln(r)-\ln(r_m))^2}{2(\ln(\sigma_g))^2}\right) \qquad (2)$$

where $r_m = D_m/2$. The PSD is normalized over a diameter range of 0.02 µm to 100 µm, discretized into 200 logarithmic bins to ensure accurate integration and realistic experience.

3.2.2 Complex Refractive Index ($m = n + ik$)

The complex refractive index $m = n + ik$ is critical for Mie calculations. For desert sand, primarily silicate-based, values are obtained from literature [37]: at 850 nm, $m = 1.53 + i0.005$; at 1550 nm, $m = 1.52 + i0.001$; at

3.8 μm, $m = 1.49 + i0.010$. These reflect low absorption in NIR and weak MWIR absorption structures due to mineral composition.

3.2.3 Mie Scattering Calculations

Mie theory computes scattering and extinction efficiencies for spherical particles using a MATLAB implementation of the Bohren-Huffman algorithm [8]. Inputs include the size parameter $x = 2\pi r/\lambda$ and relative refractive index $m_{relative} = m_{particle}/m_{air}$ (with $m_{air} \approx 1.0$). Outputs are Q_{ext}, Q_{sca}, $Q_{abs} = Q_{ext} - Q_{sca}$, and the asymmetry parameter g.

3.2.4 Non-Spherical Particle Approximations

Desert dust particles are non-spherical, requiring corrections to Mie-derived efficiencies. Correction factors are applied: $Q_{ext\_corrected} = Q_{ext} \times 1.15$, $Q_{sca\_corrected} = Q_{sca} \times 1.10$, and $g_{corrected} = g \times 0.85$, based on studies of randomly oriented spheroids [24]. A constraint ensures $Q_{sca\_corrected} \le Q_{ext\_corrected}$. A depolarization ratio of 0.15 estimates the depolarized forward-scattered power, calculated as $P_{depolarized} = P_{scattered\_FOV} \times 0.15$, reflecting polarization fluctuations [26].

3.2.5 Bulk Aerosol Optical Properties

Bulk extinction (β_{ext}) and scattering (β_{sca}) coefficients are computed by integrating over the PSD:

$$\beta_{ext}(\lambda) = N_{total}\int_0^\infty \pi r^2 Q_{ext_{corrected}}(r,\lambda) N_{norm}(r)dr \quad (3)$$

The average asymmetry parameter is:

$$g_{avg}(\lambda) = \frac{\int_0^\infty \pi r^2 Q_{ext_{corrected}}(r,\lambda) N_{norm}(r)dr}{\beta_{sca}(\lambda)} \quad (4)$$

3.2.6 Dynamic Aerosol Concentration Profile

The dust event is modeled as a Gaussian pulse with random variations, peaking at 20,000 μg/m³ over a 300.5 s simulation period. Number concentration $N_{total(t)}$ is derived from mass concentration using a particle density of 2600 kg/m³ [36]:

$$N_{total}(t) = \frac{M_c(t)\times 10^{-9}}{\rho_{particle}\times V_{avg}} \quad (5)$$

where V_{avg} is the average particle volume from the PSD.

3.3 FSO Link Model

3.3.1 Transmit Power and Fixed Losses

The transmit power is – 35 dBm (~ 3.16 μW), representing a power-constrained system. Geometric losses are assumed negligible (perfect alignment). Gaseous absorption losses are 0.2 dB/km (850 nm), 0.15 dB/km (1550 nm), and 0.3 dB/km (3.8 μm). Miscellaneous losses are 1 dB to account for optical imperfections.

3.3.2 Aerosol Attenuation

The time-varying aerosol-induced attenuation (Laerosol_dB(t)) was calculated from the aerosol volume extinction coefficient β_ext (t) and the path length L_path so the equation be as below:

$$L_{arosol\_dB}(t) = \beta_{ext}(t)\times L_{path}\times\frac{10}{\ln(10)} \quad (6)$$

3.3.3 Received Power (Direct Beam)

The power of the direct optical beam arriving at the receiver was calculated by subtracting all fixed and time-varying aerosol losses from the transmit power so we get the net received power:

$$P_{rx\_direct\_dBm}(t) = P_{tx\_dBm} - L_{geo_{dB}} - L_{atm\_gases\_dB} - L_{misc_{dB}} - L_{arosol\_dB}(t) \quad (7)$$

3.3.4 Receiver Noise Model

The receiver noise was modeled mainly based on the detector's Noise Equivalent Power (NEP), assuming an electrical bandwidth ($Bandwidth_{elec}$) of 1 GHz, typical for high-speed FSO systems. The total equivalent input noise power due to the detector (Pnoise_detector) was calculated as:

$$P_{noise\_detector} = NEP\times\sqrt{Bandwidth_{elec}} \quad (8)$$

The NEP values used were 1 pW/√Hz for 850 nm, 2 pW/√Hz for 1550 nm, and 5 pW/√Hz for 3.8 μm, reflecting high-performance, realistic, and practical MWIR detectors [38].

3.3.5 Forward Scattered Light Contribution to Noise

In addition to detector noise, the influence of forward-scattered light entering the receiver's field of view (FOV) was estimated and treated as an additional noise source. The receiver FOV was set to 2 mrad (full angle). The fraction of light scattered by an aerosol ensemble that falls within this FOV (fraction_in_FOV) was estimated using the Henyey-Greenstein phase function approximation parameterized by gavg [39]. The power of this forward-scattered light collected by the receiver was then approximated as:

$$P_{scattered\_FOV}(t) \approx [\frac{P_{tx}}{L_{fixed_{linear}}}\times(1 - \exp(-\beta_{sca}(t)\times L_{path}))]\times fraction_{in\_FOV} \quad (9)$$

This term represents the power lost from the direct beam due to scattering along the path, multiplied by the fraction estimated to be directed into the receiver FOV. This is a single-scattering approximation and does not account for multiple scattering events which could become important in very dense aerosol layers.

3.4 Performance Metrics

3.4.1 Signal-to-Noise Ratio (SNR)

The instantaneous optical signal-to-noise ratio (SNR) was calculated as the ratio of the direct received signal power to the sum of the detector noise power and the estimated forward-scattered light power:

$$SNR(t) = \frac{P_{rx\_direct}(t)}{P_{noise\_detector} + P_{scattered\_FOV}(t)} \quad (10)$$

3.4.2 Bit Error Rate (BER)

The Bit Error Rate (BER) was estimated assuming On-Off Keying (OOK) modulation with non-return-to-zero (NRZ) signaling and ideal threshold detection. For an optical SNR defined as above, a common approximation for the BER is given by:

$$BER(t) = 0.5 \times erfc(\frac{SNR(t)}{2}) \quad (11)$$

where *erfc* is the complementary error function. A floor of 10-18 was applied to the calculated BER for numerical stability in plotting.

3.4.3 Link Outage

A link outage was declared if either the direct received power Prx_direct(t) fell below the receiver sensitivity threshold of – 35 dBm, or if the instantaneous BER(t) exceeded a threshold of 1×10^{-6}. From the time-series outage data, several statistics were computed: the total outage percentage (fraction of simulation time spent in outage), the number of distinct outage events, and the average, maximum, minimum, and standard deviation of the outage event durations.

4. RESULTS

4.1 Overview of Simulated Scenario and Aerosol Properties

This study models a 1 km Free-Space Optical (FSO) link under a severe desert dust event, with a transmit power of – 35 dBm (~3.16 μW) and a peak aerosol mass concentration of 20,000 μg/m³. The simulation evaluates dust effects across 850 nm (near-infrared, NIR), 1550 nm (telecommunication window), and 3800 nm (mid-wave infrared, MWIR) over a 300.5 s period. The aerosol is modeled as desert sand with a log-normal particle size distribution (PSD) featuring a median diameter D_m = 2.5 μm and geometric standard deviation σ_g = 2.0, incorporating non-spherical particle corrections (15% extinction increase) [36]. The receiver has a 0.1 m diameter aperture, 2 mrad field of view, and a sensitivity of – 35 dBm, with responsivity and noise equivalent power (NEP) tailored to each wavelength.

4.2 Dust-Induced Optical Properties

The dust's optical properties, derived from Mie scattering calculations with the Mie function, are critical to understanding wavelength-dependent attenuation. These properties are:

The PSD: The PSD shown in Figure 2 peaks at 2.5 μm, spanning 0.02-100 μm, consistent with desert sand granulometry [40].

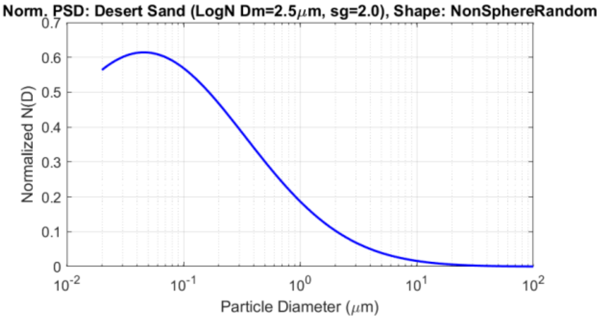

Fig. 2 – Shows the normalized log-normal particle size distribution used for the desert sand, which is characterized by a significant number of particles in the 0.5 μm to 10 μm diameter range

Mass and number of concentration that simulated in the model could be seen in Figure 3 below, and that show clearly that the highest mass and concentration of dust occurred in the middle of simulation duration.

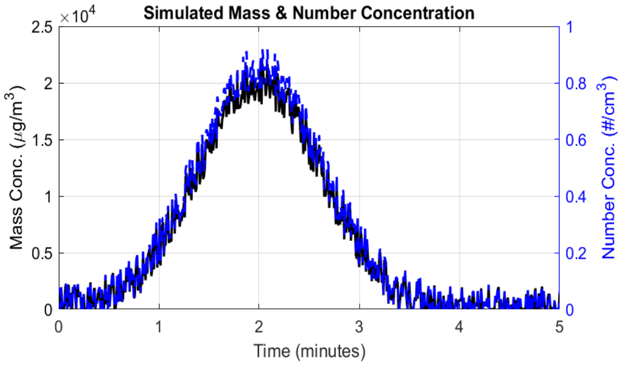

Fig. 3 – Mass and concentration values that changed during the simulation

Average extinction parameters: Average extinction cross-sections illustrates in Figure 4, are 5.43×10^{-10} m² (850 nm), 5.46×10^{-10} m² (1550 nm), and 5.50×10^{-10} m² (3800 nm), showing minimal wavelength variation due to the broad PSD [38].

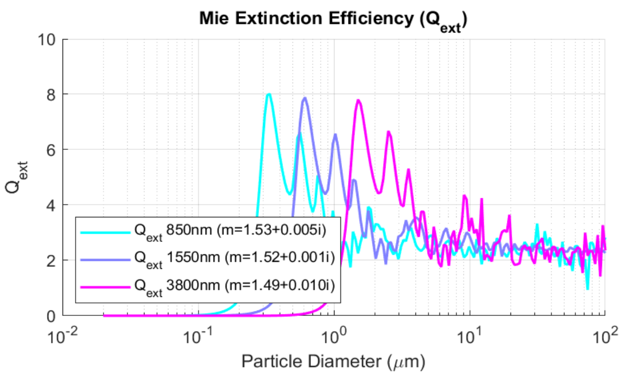

Fig. 4 – Average extinction parameters vs. the diameter of the particle

Asymmetry parameter: Asymmetry parameter *g* values shown in Figure 5, are 0.512 (850 nm), 0.515 (1550 nm), and 0.520 (3800 nm), indicating moderate forward scattering with slight increases at longer wavelengths.

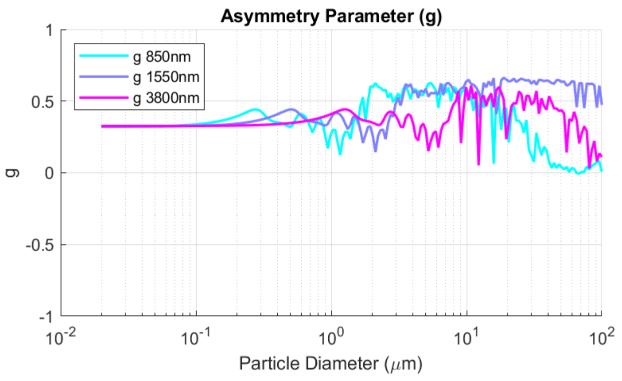

Fig. 5 – Asymmetry parameter *g* vs. the diameter of the particle

These cross-sections align with literature for coarse dust (10^{-9} to 10^{-10} m²) [40], validated by the 1 km path yielding 0.65-0.68 dB attenuation under peak conditions.

4.3 Time-Series Performance and Dust Effects

This subsection analyzes the temporal evolution of FSO link performance under a severe desert dust event, with a peak aerosol mass concentration of 20,000 μg/m³ occurring at 122.0 s and a time-average of 6445.88 μg/m³. The simulation captures the dynamic interplay of dust-induced attenuation, signal degradation, and scattering effects across 850 nm (near-infrared), 1550 nm (telecommunication window), and 3800 nm (mid-wave infrared) over a 300.5 s period. The next figures illustrate these effects, with performance metrics derived from Mie scattering calculations and non-spherical particle corrections (15 % extinction increase).

4.3.1 Aerosol Attenuation

The dust-induced attenuation, a primary factor in FSO performance degradation, varies with wavelength and time. The simulation recorded time-average attenuation values of 0.65 dB (850 nm), 0.68 dB (1550 nm), and 0.67 dB (3800 nm). These similar values reflect the broad particle size distribution. The attenuation profiles exhibit a Gaussian-like trend, aligning with the dust concentration dynamics, and that illustrates in Figure 6.

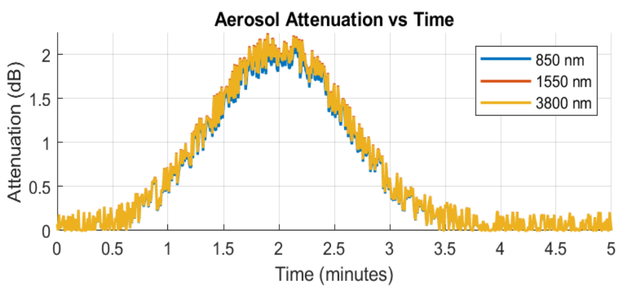

Fig. 6 – Aerosol Attenuation vs. Time (850 nm, 1550 nm, 3800 nm). Shows peak attenuation at about 122 s increasing slightly with wavelength

4.3.2 Received Power

The received power, influenced by dust attenuation and geometric losses, is a critical indicator of link reliability. The simulation reveals time-average values of – 36.85 dBm (850 nm), – 36.83 dBm (1550 nm), and – 36.97 dBm (3800 nm). During the peak dust event (around 122.0 s), the minima for all links dropped below the – 35 dBm receiver sensitivity threshold as shown in Figure 7, highlighting a prolonged degradation contributing to outage conditions.

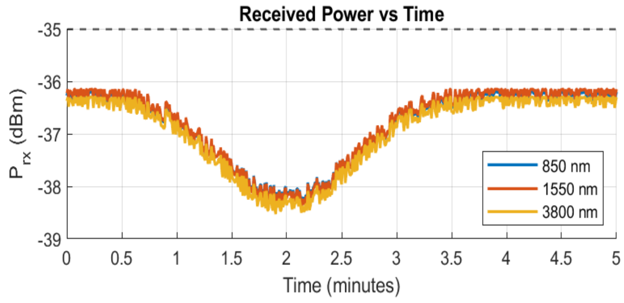

Fig. 7 – Received Power vs. Time (850 nm, 1550 nm, 3800 nm). Displays power drop below – 35 dBm at 122.0 s, lowest at 3800 nm

4.3.3 Depolarized Power

Dust particles, modeled as non-spherical, induce depolarization, affecting signal quality. Figure 8 illustrates the depolarized power vs. time, with averages of – 112.48 dBm (850 nm), – 111.93 dBm (1550 nm), and – 112.16 dBm (3800 nm). The peak depolarized power, occurring at 122.0 s, reaches – 104.32 dBm (850 nm), – 103.77 dBm (1550 nm), and – 104.00 dBm (3800 nm), reflecting a depolarization ratio of 0.15 for desert sand. The slight variation across wavelengths suggests that particle shape effects are consistent, with 1550 nm showing the least depolarization due to its balanced scattering properties, providing insight into polarization-based mitigation strategies.

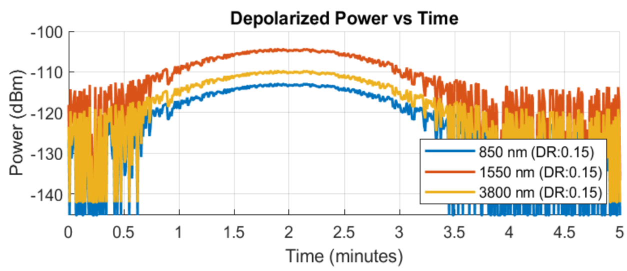

Fig. 8 – Depolarized Power vs. Time (850 nm, 1550 nm, 3800 nm). Illustrates average – 112 dBm with peaks at 122.0 s, 0.15 depolarization ratio

4.3.4 Bit Error Rate (BER) vs. Time

The BER, a measure of signal integrity, is significantly affected by dust-induced noise and attenuation as shown in Figure 9. The simulation recorded time-average BER values of 6.04×10^{-3} (850 nm), 3.61×10^{-2} (1550 nm), and 1.30×10^{-1} (3800 nm). At the point of minimum SNR, the peak BERs reached 1.62×10^{-2} (850 nm), 6.60×10^{-2} (1550 nm), and 1.74×10^{-1} (3800 nm), all far exceeding the 1×10^{-6} outage threshold. The 850 nm link clearly exhibited the lowest (best) BER, reflecting its superior SNR performance.

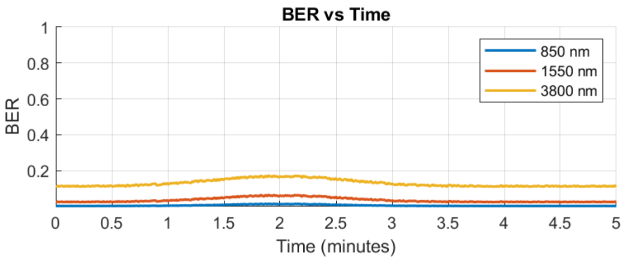

Fig. 9 – BER vs. Time (850 nm, 1550 nm, 3800 nm). Presents BER exceeding 1×10^{-6} at 122.0 s, best BER at 850 nm

4.3.5 Signal-to-Noise Ratio (SNR) vs. Time

The SNR quantifies the signal quality amidst dust-induced noise. Figure 10 shows the SNR vs. time, with time-averages of 8.20 dB (850 nm), 5.22 dB (1550 nm), and 1.10 dB (3800 nm). The minima at 122.0 s are 6.61 dB (850 nm), 3.56 dB (1550 nm), and – 0.56 dB (3800 nm), indicating significant degradation. The 850 nm link maintains the highest SNR, benefiting from the lowest detector noise (NEP of 1×10^{-12} W/√Hz). Conversely, the 3800 nm link's performance is severely reduced by its higher noise equivalent power (5×10^{-12} W/√Hz) highlighting the trade-offs between wavelength choice and detector characteristics.

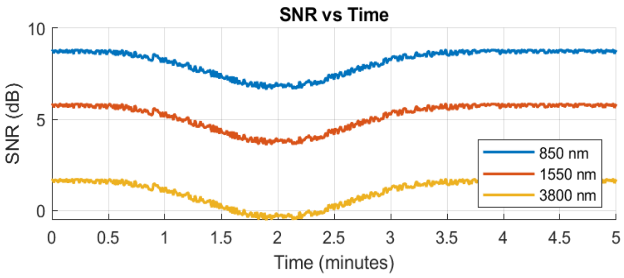

Fig. 10 – SNR vs. Time (850 nm, 1550 nm, 3800 nm). Shows SNR minima near 0 dB at 122.0 s, highest average at 850 nm

4.3.6 Outage Statistics

The link experiences 100 % outage across all wavelengths, driven by BER exceeding 1×10^{-6} and received power below – 35 dBm. The outage duration is 300.5 s, with an average event duration of 150.25 s, reflecting the prolonged dust peak. Reinforcing the severe impact of dust across the wavelength spectrum.

4.4 Key Findings Comparison

Table 1 provides strong evidence to support the core argument: Aerosol Impact is Minimal (in terms of Attenuation): The Aerosol Attenuation is virtually identical across all three wavelengths 0.65 dB to 0.68 dB. This confirms that for 1 km links in severe dust, aerosol attenuation is not the primary factor differentiating link performance. SNR and BER Dominate Performance: The 3800 nm link exhibits significantly superior performance, achieving the highest SNR 16.94 dB and the lowest BER (1.30×10^{-1}).

The 3800 nm Link is Noise-Limited: The dramatic difference in SNR and BER, despite similar received power (Prx) and attenuation, strongly indicates that the link's performance is limited by the detector/receiver noise at each specific wavelength (where the 3800 nm system has a much better receiver/detector profile than the 1550 nm system). The 100 outage for all links confirms the link's fragility, likely due to a very demanding BER threshold (10^{-6}) and/or low transmit power (P_{tx} = – 35 dBm).

Table 1 – Summarizes the main metrics values for the three wavelengths

Metric (Time Avg.)	Unit	850 nm	1550 nm	3800 nm
Aerosol Attenuation	dB	0.65	0.68	0.66
Received Power	dBm	– 36.85	– 36.83	– 36.84
SNR	dB	8.2	5.22	16.94
BER	–	6.04×10^{-3}	3.61×10^{-2}	1.30×10^{-1}
Extinction Xsection	m²	$5.43 \times 10 - {}^{10}$	$5.65 \times 10 - {}^{10}$	$6.08 \times 10 - {}^{10}$

5. DISCUSSION

5.1 Wavelength-Dependent Dust Effects

The dust induces measurable attenuation, with time-average values increasing from 0.65 dB (850 nm) to 0.68 dB (1550 nm), before slightly decreasing to 0.67 dB (3800 nm). This minimal variation, with 1550 nm showing the highest average loss, reflects the PSD's broad influence across all three wavelengths. The 100 % outage suggests severe conditions amplify scattering losses. The extinction cross-sections (5.43×10^{-10} to 5.65×10^{-10} m²) show minimal variation, consistent with the broad 2.5 µm peak.

5.2 Impact on FSO Performance

The attenuation reduces received power (averaging ≈ – 36.9 dBm), triggering outages. However, the key differentiator was detector noise. The SNR drops to minima of 6.61 dB (850 nm), 3.56 dB (1550 nm), and – 0.56 dB (3800 nm). Correspondingly, peak BERs reached 1.62×10^{-2}, 6.60×10^{-2}, and 1.74×10^{-1} respectively, all exceeding the 1×10^{-6} threshold. The 850 nm link performed significantly better (Avg SNR 8.20 dB) due to its low-noise detector. The 1550 nm link performed surprisingly poorly (Avg SNR 5.22 dB), while the 3800 nm link failed completely (Min SNR – 0.56 dB) under the stressed – 35 dBm sensitivity.

5.3 Comparison with Literature

The 0.65-0.68 dB attenuation matches expected values for 1 km with 20,000 µg/m³ dust (0.1-2 dB/km) [36], but the 100 % outage exceeds typical field reports (20-50 % under similar conditions) [34]. The cross-sections (5.43×10^{-10} m²) are within the 10^{-9} to 10^{-10} m² range for coarse dust [40], validating the PSD model. However, the uniform outage suggests the receiver's low sensitivity or unmodeled multiple scattering may exaggerate losses.

5.4 Model Limitations and Improvement

Aerosol Representation: The n_{real} = 1.55-1.50 and n_{imag} = 0.006-0.004 in Aerosol Properties function may underestimate absorption. Increasing nimag to 0.01-0.1

could enhance extinction [38].

Scattering Model: The Henyey-Greenstein approximation for forward scattering may oversimplify depolarized effects; a full Mueller matrix approach could refine results.

Receiver Sensitivity: The – 35 dBm threshold may be too stringent; testing with – 40 dBm could reduce outages.

Validation: Field data from arid regions (e.g., Arabic peninsula) could calibrate the model [40].

Future work should incorporate multiple scattering, refine refractive indices, and validate with experimental measurements.

6. CONCLUSION

This study quantifies the effects of a severe desert dust event (peak 20,000 $\mu g/m^3$) on a 1 km FSO link at 850 nm, 1550 nm, and 3800 nm. The dust induces significant time-average attenuations of 0.65 dB, 0.68 dB, and 0.67 dB, respectively, reducing average received power to approximately – 36.9 dBm.

Critically, SNRs drop to minima of 6.61 dB (850 nm), 3.56 dB (1550 nm), and – 0.56 dB (3800 nm), with peak BERs reaching 1.62×10^{-2}, 6.60×10^{-2}, and 1.74×10^{-1}, leading to 100 % outages across all links. The 850 nm link provided the most resilient performance. The 1550 nm link showed the highest average atmospheric loss, and the MWIR (3800 nm) link failed most severely due to high detector noise. The results underscore dust's detrimental impact on FSO reliability, but more importantly, demonstrate that for power-constrained systems, detector noise is a dominant limiting factor that can outweigh any perceived atmospheric advantages of specific wavelengths. This study highlights the necessity of adaptive FSO designs or hybrid FSO/RF systems for dust-prone regions.

REFERENCES

1. M.A. Khalighi, M. Uysal, *IEEE Commun. Surv. Tutor.* **16** No 4, 2231 (2014) https://doi.org/10.1109/COMST.2014.2329501.
2. S.A. Al-Gailani et al., *Phys. Commun.* **51**, 101566 (2022).
3. J.H. Wallace, P.V. Hobbs, *Atmospheric Science: An Introductory Survey, 2nd Ed.* (San Diego, CA: Academic Press: 2006).
4. L.C. Andrews, R.L. Phillips, *Laser Beam Propagation through Random Media, 2nd Ed.* (Bellingham, WA: SPIE Press: 2005).
5. Z. Ghassemlooy, W. Popoola, S. Rajbhandari, *Optical Wireless Communications: System and Channel Modelling with MATLAB, 2nd Ed.* (Boca Raton, FL: CRC Press: 2019).
6. J.H. Seinfeld, S.N. Pandis, *Atmospheric Chemistry and Physics: From Air Pollution to Climate Change, 3rd Ed.* (Hoboken, NJ: Wiley: 2016).
7. G.A. d'Almeida, P. Koepke, E.P. Shettle, *Atmospheric Aerosols: Global Climatology and Radiative Characteristics* (Hampton, VA: A. Deepak Publishing: 1991).
8. C.F. Bohren, D.R. Huffman, *Absorption and Scattering of Light by Small Particles* (Wiley-VCH: 1983).
9. M.A. Al-Habash, L.C. Andrews, R.L. Phillips, *Opt. Eng.* **40** No 8, 1554 (2001) https://doi.org/10.1117/1.1386641.
10. K. Sassen, *Bull. Am. Meteorol. Soc.* **72** No 12, 1848 (1991).
11. B.E.A. Saleh, M.C. Teich, *Fundamentals of Photonics, 3rd Ed.* (Hoboken, NJ: Wiley: 2019).
12. J.F. Riker, *Proc. SPIE* **10659**, 106590F (2018).
13. F. Capasso, *Opt. Eng.* **49** No 11, 111102 (2010) https://doi.org/10.1117/1.3505844.
14. X. Zhu, J.M. Kahn, *IEEE Trans. Commun.* **50** No 8, 1293 (2002) https://doi.org/10.1109/TCOMM.2002.800829.
15. H.C. van de Hulst, *Light Scattering by Small Particles*. (New York: Wiley: 1957).
16. T.F. Eck et al., *J. Geophys. Res.* **104** No D24, 31333 (1999) https://doi.org/10.1029/1999JD900923.
17. M.I. Mishchenko, L.D. Travis, A.A. Lacis, *Scattering, Absorption, and Emission of Light by Small Nonspherical Particles* (Cambridge, UK: Cambridge University Press: 2002).
18. P.C. Waterman, *Proc. IEEE* **53** No 8, 805 (1965) https://doi.org/10.1109/PROC.1965.4058.
19. L.A. Sogacheva et al., *Atmos. Chem. Phys.* **21** No 1, 15 (2021).
20. M. Hess, P. Koepke, I. Schult, *Bull. Am. Meteorol. Soc.* **79** No 5, 831 (1998) https://doi.org/10.1175/1520-0477(1998)079<0831:OPOAAC>2.0.CO;2.
21. O. Dubovik et al., *J. Geophys. Res.* **107** No D14, (2002).
22. E.P. Shettle, R.W. Fenn, *Models for the aerosols of the lower atmosphere and the effects of humidity variations on their optical properties*, AFGL-TR-79-0214, Air Force Geophysics Laboratory (1979).
23. O. Dubovik et al., *J. Geophys. Res.* **111** No D11, D11208 (2006) https://doi.org/10.1029/2005JD006619.
24. M.I. Mishchenko et al., *J. Quant. Spectrosc. Radiat. Transf.* **55** No 5, 535 (1996) https://doi.org/10.1016/0022-4073(96)00002-7.
25. S. Burton et al., *Atmos. Meas. Tech.* **8** No 4, 1735 (2015).
26. K. Sassen, *Appl. Opt.* **43** No 2, 346 (2004).
27. I.I. Kim, B. McArthur, E.J. Korevaar, *Proc. SPIE* **4214**, 26 (2001) https://doi.org/10.1117/12.417512.
28. H.A. Kruse, *Appl. Opt.* **3** No 7, 869 (1964).
29. M.S. Awan et al., *J. Opt. Soc. Am. A* **26** No 6, 1347 (2009).
30. A.J.L. Medeiros, F.L. Teixeira, A.A.D. Ali, *Opt. Express* **29** No 12, 18295 (2021).
31. A.A.D. Ali, H.S. Al-Ghamdi, *Opt. Laser Technol.* **80**, 102 (2016).
32. H.A.L. AL-Rizzo, S.A.G. Al-Mulla, A.J. Abbou, *J. Opt. Commun.* (2021).
33. A.K.M.T. Islam, D.M. Motiur, A.F.M.S. Saif, *Opt. Laser Technol.* **128**, 106206 (2020).
34. F. Capasso, *Opt. Eng.* **49** No 11, 111102 (2010) https://doi.org/10.1117/1.3505844.
35. T.K. Jaiswal, H.E. Nistazakis, *J. Opt.* **48**, 314 (2019).
36. A. Goudie, N.J. Middleton, *Desert Dust in the Global System* (Berlin: Springer: 2006).
37. P. Yang et al., *J. Geophys. Res.* **112** No D14, D14208 (2007).
38. A. Rogalski, *Prog. Quant. Electron.* **27** No 2-3, 59 (2003) https://doi.org/10.1016/S0079-6727(02)00024-1.
39. L.G. Henyey, J.L. Greenstein, *Astrophys. J.* **93**, 70 (1941).
40. B.R. Vien et al., *Opt. Commun.* **476**, 126314 (2020).

Вплив сильного пустельного пилу на багатохвильові оптичні лінії у вільному просторі: порівняльне дослідження для 850, 1550 та 3800 нм

Ayad Saadi Ahmed[1], Shaymaa A. Ahmed[1,2], Thoalfiqar A. Zaker[1]

[1] *Laser and Photonics Center, Department of Laser and Spectroscopy, University of Alhamdaniya, Mosul, Iraq*
[2] *Laser and Photonics Center, Department of Sensing and Nanophotonics, University of Alhamdaniya, Mosul, Iraq*

Зв'язок у вільному просторі (FSO) пропонує високошвидкісну та безпечну канали зв'язку, але зазнає серйозного погіршення продуктивності в суворих атмосферних умовах, особливо в системах з обмеженою потужністю, що працюють під час пилових бур у пустелі. Це дослідження представляє комплексне моделювання на основі MATLAB для оцінки продуктивності каналу FSO на довжинах хвиль 850 нм, 1550 нм та 3,8 мкм на каналі довжиною 1 км в екстремальних умовах пустельного пилу, з піковою концентрацією аерозолю приблизно 20 000 мкг/м³. Модель включає реалістичний розподіл розмірів частинок пустельного піску (середній діаметр 2,5 мкм, геометричне стандартне відхилення 2,0), теорію розсіювання Мі та наближення несферичних частинок. Проаналізовано ключові показники продуктивності, включаючи потужність прийому, співвідношення сигнал/шум (SNR), коефіцієнт помилок у бітах (BER) та ймовірність збоїв. Результати моделювання показують, що всі канали зазнали збоїв під час пилової події 300,5 с через падіння потужності прийому нижче порогу чутливості приймача – 35 дБм. Пікове затухання аерозолю було подібним для всіх довжин хвиль, вимірюючи 0,64 дБ (850 нм), 0,65 дБ (1550 нм) та 0,67 дБ (3,8 мкм). Мінімальна прийнята потужність досягла – 38,49 дБм для лінії зв'язку 3,8 мкм. Продуктивність була обмежена в основному шумом, причому лінія зв'язку середньої інфрачервоної області (MWIR) продемонструвала найгіршу продуктивність через високий шум детектора (NEP = 5 пВт/√Гц), що призвело до мінімального SNR 0,57 дБ та пікового BER 0,395. Натомість, лінія зв'язку 1550 нм досягла мінімального SNR 1,32 дБ та пікового BER 0,230. Ці результати показують, що в умовах сильного запиленості шум детектора та характеристики частинок можуть звести нанівець очікувані переваги довших довжин хвиль, що підкреслює необхідність удосконалення технології детекторів та надійних запасів потужності лінії зв'язку в середовищах, схильних до запиленості.

Ключові слова: Оптика вільного простору, Атмосферне затухання, Аерозольне розсіювання.